Journal of Constructional Steel Research 158 (2019) 405–416

Contents lists available at ScienceDirect

Journal of Constructional Steel Research

Experimental and numerical investigations of concrete-filled stainless steel tube stub columns under axial partial compression

An He, Ou Zhao *

School of Civil and Environmental Engineering, Nanyang Technological University, Singapore

ARTICLE INFO

Article history:
Received 29 November 2018
Received in revised form 6 March 2019
Accepted 3 April 2019
Available online 11 April 2019

Keywords:
Concrete-filled stainless steel tube (CFSST)
Design standards
New design proposal
Numerical simulation
Partial compression tests
Stub column

ABSTRACT

This paper presents a thorough experimental and numerical investigation into the structural performance and load-carrying capacities of circular concrete-filled stainless steel tube (CFSST) stub columns under axial partial compression. The experimental programme was carried out on 3 fully loaded (reference) circular CFSST stub column specimens and 15 partially loaded circular CFSST stub column specimens, with a series of material and geometric parameters (including the concrete grade, the stainless steel tube size and the area and shape of the partial compression region) varied. Analysis of the obtained test results revealed that the partial compression area ratio, defined as the ratio of the concrete gross area to the partially loaded area, and the confinement factor, given as the steel tube to concrete plastic compression resistance ratio, are the two key factors influencing the structural behaviour and load-carrying capacities of circular CFSST stub columns subjected to partial compression. The testing investigation was supplemented by a systematic finite element (FE) modelling study, where the numerical models were firstly developed and validated against the experimentally derived results and then employed to conduct parametric studies for the purpose of expanding the experimental data pool over a broader range of partial compression area ratios and confinement factors. In the absence of the established codified design provisions for CFSST stub columns subjected to partial compression, the corresponding design rules for partially loaded concrete-filled carbon steel tube stub columns, as given in the European code and American specification, were evaluated for CFSST stub columns under partial compression load, and shown to result in both conservative and scattered resistance predictions. Other recently developed proposals for partially loaded concrete-filled carbon steel tube stub columns were also assessed for CFSST stub columns, indicating a high level of design accuracy on average but with many unsafe resistance predictions. Finally, a new design approach was developed specifically for CFSST stub columns under partial compression, and shown to yield precise, consistent and safe-sided resistance predictions through comparing against the test and FE results.

1. Introduction

Concrete-filled steel tube (CFST) columns have been extensively utilised as vertical load-bearing components in high-rise buildings and bridges. In comparison with the conventional bare steel and reinforced concrete columns, CFST columns possess higher load-carrying capacity, larger stiffness and better seismic behaviour. This can be primarily attributed to the beneficial composite action developed between the outer steel tube and the inner concrete core; the outer steel tube provides lateral confinement to the inner concrete core, leading to an increase in concrete strength and ductility in the axial direction, while the inner concrete core restrains the inward deformation of the outer steel tube and thus delays its occurrence of local buckling. The past decade has witnessed an increasing trend of using stainless steel tubes to replace carbon steel tubes in the fabrication of CFST structural members, principally due to the excellent durability and mechanical properties of stainless steel. Compared to carbon steel, stainless steel has (i) significantly better corrosion resistance, requiring little or no maintenance work during the service life, and (ii) much higher level of ductility and strain hardening, leading to composite members with more ductile structural behaviour and more flat post-ultimate response. A brief summary of the previous research on concentrically loaded concrete-filled stainless steel tube (CFSST) column members is described as follows. Stub column tests on normal strength concrete-filled stainless steel tubes of different shapes (e.g., square [1–3], rectangular [2,3] and circular [1,3]) have been performed to study their compression resistances as well as the lateral confinements provided by stainless steel tubes of different shapes to concrete. The compressive behaviour and strengths of novel recycled aggregate concrete-filled stainless steel tube stub columns were experimentally investigated by Yang and Ma [4], while Li et al. [5,6] performed axial compression tests on CFST stub columns with the concrete infill made of seawater and sea sand. The flexural (global) buckling behaviour of normal strength and fibre reinforced

* Corresponding author.
E-mail address: ou.zhao@ntu.edu.sg (O. Zhao).

https://doi.org/10.1016/j.jcsr.2019.04.002

concrete-filled stainless steel tube long columns was experimentally investigated by Uy et al. [1] and Ellobody and Ghazy [7], respectively, where the effects of a series of material and geometric parameters, including the concrete strength, stainless steel tube size and member slenderness ratio, on the buckling strengths of CFSST long columns were quantified. Han et al. [8] and Tao et al. [9] performed fire tests on normal strength concrete-filled stainless steel tube long columns, to study their structural behaviour at elevated temperatures, while the post-fire tests on normal strength concrete-filled stainless steel tube stub columns were carried out by Chen et al. [10]. Although there have been extensive experimental investigations into the static, fire and post-fire performance of CFSST column members, to date, their behaviour under partial compression (i.e. the axial compression load acts only on the middle portion of the concrete infill of CFSST column) remains unexplored, and is thus the subject of the present study. The loading case of partial compression is common in bridge and structural engineering applications; for example, piers supporting beam girders of bridges through bearings and columns holding up arch structures through bearings are subjected to partial compression load.

The structural behaviour and load-carrying capacities of circular CFSST stub columns under partial compression was investigated in this paper, on the basis of a systematic testing and numerical simulation programme. The experimental study was carried out on 15 partially loaded circular CFSST stub column specimens and 3 fully loaded (reference) circular CFSST stub column specimens, while finite element models were developed in the numerical simulation programme to replicate the test results of the partially and fully loaded circular CFSST stub column specimens, and to carry out parametric studies to expand the experimental data pool over a broader range of stainless steel tube sizes and partial compression areas. Given that there have been no established design standards for stainless steel–concrete composite structures, the applicability of the corresponding design rules for concrete-filled carbon steel tube stub columns under partial compression, as given in the European code EN 1994-1-1 [11] and American specification AISC 360-16 [12] and proposed in Han et al. [13], to partially loaded CFSST stub columns was assessed, based on the derived test and numerical data. Finally, An improved design approach for CFSST stub columns under partial compression was developed.

2. Experimental study

2.1. Test specimens

A total of 18 circular CFSST stub column specimens, with 15 under partial compression and 3 subjected to full compression, were considered in the present testing. Two cold-formed grade EN 1.4301 austenitic stainless steel circular hollow section (CHS 73 × 3 and CHS 89 × 3) tubes were utilised to fabricate the CFSST stub column specimens. Specifically, for the austenitic stainless steel CHS 73 × 3 tubes, concrete infill of two grades (C50 and C60) was employed, and both circular and square bearing plates were adopted for the application of partial compression load, leading to a total of four series of partially loaded CFSST stub column specimens, namely D73-C50-C, D73-C50-S, D73-C60-C, D73-C60-S, while an additional series of CFSST stub column specimens (D89-C60-C) was fabricated from the austenitic stainless steel CHS 89 × 3 tubes and C60 concrete, and tested using circular bearing plates. Note that the labelling system of each partially loaded CFSST stub column specimen series starts with a letter 'D' (indicating diameter) and the nominal outer diameter of the stainless steel tube, followed by the grade of the concrete infill, and ends with a letter 'C' or 'S' (identifying circular or square shape of the partial compression region), e.g., D73-C50-C. For each of the five specimen series, three partial compression areas, achieved through the use of square (or circular) bearing plates with varying sizes, were examined in the testing, resulting in a total of 15 partially loaded CFSST stub columns. The employed identifier code for each specimen comprises the ID of the specimen series and a number, with '1–3' signifying various partial compression areas, e.g., D73-C50-C-2. The designed specimens allowed the effects of a range of material and geometric parameters, including the concrete strength, the stainless steel tube size, and the shape and area of the partial compression region, on the behaviour and strengths of partially loaded circular CFSST stub columns to be investigated. Table 1 reports the measured geometric dimensions of the CFSST stub column specimens and the bearing plates employed for partial compression tests, where D and t are respectively the outer diameter and thickness of the austenitic stainless steel tube, L is the length of the stub column specimen, d_b is the diameter of the circular bearing plate, b_b is the width of the square bearing plate, t_b is the bearing plate thickness, A_s, A_c and A_b are the areas of the outer austenitic stainless steel tube, inner concrete core and bearing plate, respectively, and β is the partial compression area ratio and defined as the area ratio of the inner concrete core to the bearing plate, i.e. $\beta = A_c/A_b$. The key geometric dimensions of the three fully loaded (reference) circular CFSST stub column specimens (denoted as D73-C50, D73-C60 and D89-C60) are also reported in Table 1.

2.2. Material testing

The material properties of the austenitic stainless steel CHS tubes were measured through tensile coupon tests. For each circular hollow section size, two longitudinal coupons were cut at 90 degrees from

Table 1
Measured geometric properties of partially and fully loaded CFSST stub column specimens.

Specimen	D (mm)	t (mm)	L (mm)	d_b (mm)	b_b (mm)	t_b (mm)	A_s (mm^2)	A_c (mm^2)	A_b (mm^2)	β	ξ
D73-C50	72.8	2.85	215	–	–	–	626	3534	–	–	0.9
D73-C50-C-1	72.9	2.79	216	67	–	30	614	3552	3524	1.0	0.9
D73-C50-C-2	72.8	2.78	216	51	–	62	611	3544	2042	1.7	0.9
D73-C50-C-3	73.3	2.79	216	35	–	33	617	3595	962	3.7	0.9
D73-C50-S-1	73.0	2.83	214	–	45	64	623	3560	1980	1.8	0.9
D73-C50-S-2	73.0	2.84	215	–	38	40	625	3559	1444	2.5	0.9
D73-C50-S-3	73.0	2.84	216	–	25	37	625	3559	625	5.7	0.9
D73-C60	72.8	2.84	216	–	–	–	624	3536	–	–	0.7
D73-C60-C-1	73.5	2.77	216	67	–	30	616	3625	3524	1.0	0.7
D73-C60-C-2	73.0	2.80	216	51	–	62	616	3567	2042	1.7	0.7
D73-C60-C-3	73.3	2.84	217	35	–	33	628	3584	962	3.7	0.7
D73-C60-S-1	72.8	2.80	215	–	45	64	616	3539	1980	1.8	0.7
D73-C60-S-2	72.8	2.85	216	–	38	40	625	3535	1444	2.5	0.7
D73-C60-S-3	72.8	2.82	216	–	25	37	619	3542	625	5.7	0.7
D89-C60	89.3	3.12	266	–	–	–	844	5416	–	–	0.8
D89-C60-C-1	89.3	3.15	266	83	–	33	852	5401	5408	1.0	0.8
D89-C60-C-2	89.5	3.13	265	64	–	38	848	5440	3165	1.7	0.8
D89-C60-C-3	89.3	3.12	265	41	–	58	844	5409	1320	4.1	0.8

Fig. 1. Test coupon test rig.

the weld [14,15], and tested using a 50 kN Universal Testing Machine, with the test rig depicted in Fig. 1, where a pair of strain gauges are affixed to both sides of the coupon at mid-height to measure the longitudinal strains, and an extensometer with 50 mm gauge length is mounted onto the middle parallel portion of the coupon to record the elongation within the gauge length. Displacement-controlled loading scheme was employed in the tensile coupon tests, with the initial rate of 0.05 mm/min up to the material nominal 0.2% proof stress, followed by a higher rate equal to 0.8 mm/min until failure of the tensile coupon [16–19]. Table 2 reports the key average measured material properties for each circular hollow section size, in which E is the Young's modulus, $\sigma_{0.2}$ is the 0.2% proof stress, σ_u and ε_u are respectively the ultimate stress and strain, and n and m are the coefficients utilised in the Ramberg–Osgood material model [20–24] to characterise the strain hardening behaviour of stainless steel, while the measured stress–strain curves for both cross-section sizes are displayed in Fig. 2.

Concretes of two grades, namely C50 and C60, were adopted in the fabrication of CFSST stub column specimens. The concretes were produced using CEM I 52.5 N Portland cement, river sand, gravel with the maximum aggregate size of 10 mm, and fresh water, with the detailed mix designs given in Table 3. For each concrete grade, three concrete cylinders were casted, and then tested at the time of the partially and fully loaded CFSST stub column tests. The average measured cylinder strengths for the C50 and C60 concretes were 49.9 MPa and 63.6 MPa, with the coefficients of variation (COVs) of 0.010 and 0.027, respectively. Upon determination of the material strengths of stainless steel and concrete, the confinement factor ξ [1,25], which is an overall measure of the lateral confinement provided by the outer stainless steel tube to the inner concrete core, can be calculated by Eq. (1) for each CFSST stub column specimen, in which $\sigma_{0.2}$ is the 0.2% proof stress of

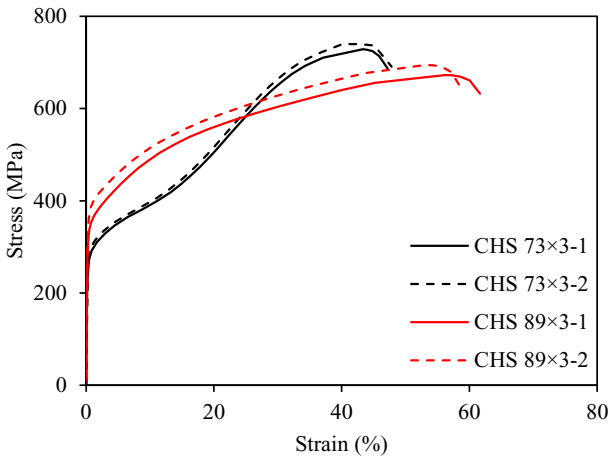

(a) Stress–strain curves

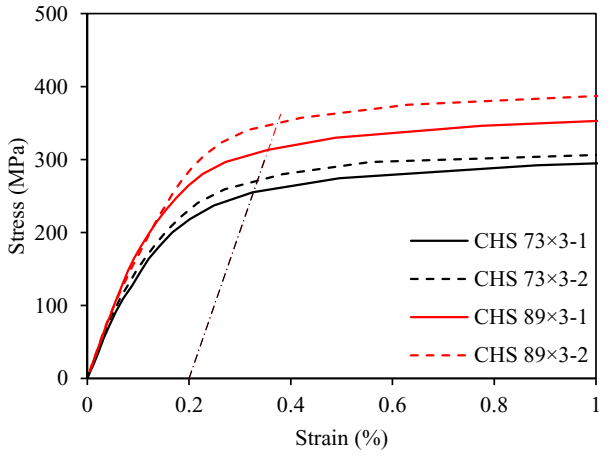

(b) Determination of 0.2% proof stress

Fig. 2. Measured material stress–strain curves of stainless steel tubes.

the stainless steel tube, f_c is the concrete cylinder strength, and A_s and A_c are respectively the areas of the stainless steel tube and concrete infill, as reported in Table 1.

$$\xi = \frac{\sigma_{0.2} A_s}{f_c A_c} \tag{1}$$

2.3. Stub column tests under partial and full compression

Partial and full compression tests on CFSST stub columns were performed utilising a displacement-controlled 2000 kN Universal Testing Machine at a speed of 0.2 mm/min. Prior to the structural testing, a thin layer of gypsum was applied to both ends of the CFSST stub column specimens and then hardened between two flat rigid platens under a small load of 5 kN; this led to the achievement of flat end surfaces of the specimens. In fully loaded stub column tests, the axial compression load was applied through two rigid platens (with the size larger than the cross-section sizes of the specimens) to both ends of the CFSST stub columns

Table 2
Key average measured material properties of stainless steel tubes.

Cross-section	E (GPa)	$\sigma_{0.2}$ (MPa)	σ_u (MPa)	ε_u (%)	n	m
CHS 73 × 3	202	258	729	43	3.8	2.2
CHS 89 × 3	201	321	673	56	4.9	2.7

Table 3
Mixture proportion of concrete.

Concrete grade	Gravel (kg)	Sand (kg)	Cement (kg)	Water (kg)
C50	795	789	462	240
C60	795	789	538	215

(a) Photograph

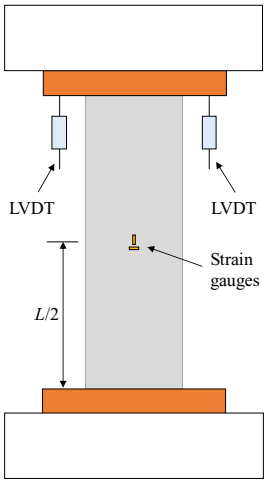

(b) Schematic diagram

Fig. 3. Test setup for fully loaded CFSST stub columns.

(a) Photograph

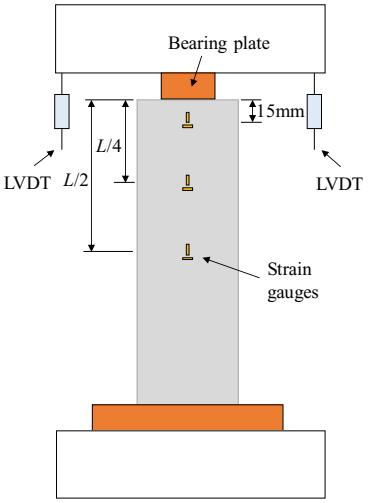

(b) Schematic diagram

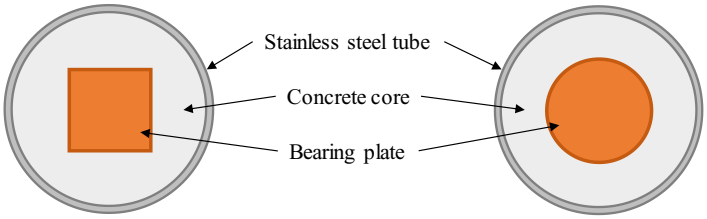

(c) Schematic plan view of partial compression loading.

Fig. 4. Test setup for partially loaded CFSST stub columns.

(see Fig. 3), allowing full compression on the end sections of the specimens to be achieved, while for partially loaded stub column tests, the top rigid platen was replaced by square or circular bearing plates (with the areas less than those of the inner concretes of the specimens, as reported in Table 1), for the application of loading, as shown in Fig. 4; this led to the top ends of the CFSST stub columns under partial compression and the bottom ends subjected to full compression, which was similar to the actual loading distribution within bridge piers, where the top and bottom ends are under partial and full compression, respectively.

Fig. 4 depicts the test rig for partially loaded CFSST stub columns, where four LVDTs are positioned at one end to record the axial deformation (end shortening) of the specimen and three pairs of orthogonal strain gauges are placed at distances of 15 mm, $L/4$ and $L/2$ (L is the specimen length) from the top end of the specimen to derive the longitudinal and transverse strains at these three positions; the strain gauge readings were adopted to derive the longitudinal and transverse strain distributions of the outer stainless steel tubes along the member length direction for CFSST stub columns under partial compression. The test setup for full loaded CFSST stub columns, as displayed in Fig. 3, is similar to that for the corresponding partially loaded specimens, except that only one pair of orthogonal strain gauges is affixed to the mid-height of the specimen.

The experimentally derived load–axial end shortening curves for the five series of CFSST stub column specimens subjected to partial compression are shown in Fig. 5(a)–(e), together with the corresponding load–deformation histories of the fully loaded (reference) specimens. Table 4 reports the experimental ultimate loads for CFSST stub columns under partial and full compression ($N_{u,p}$ and $N_{u,f}$, respectively), together with the relative capacity index (RCI), which is defined in Eq. (2) and is a measure of the loss of load-carrying capacities of partially loaded CFSST stub columns (as compared with the reference capacities of their fully loaded counterparts). Note that for partially and fully loaded CFSST stub columns with relatively flat load–deformation responses, the experimental ultimate loads ($N_{u,p}$ and $N_{u,f}$) were taken as the loads where the tangent stiffnesses of the load-end shortening curves were equal to 1% of the initial stiffnesses [26]. Figs. 6 and 7 show the failure modes for typical partially loaded CFSST stub column specimens D73-C50-C-3 and D73-C50-S-2 with circular and square partial compression regions, respectively, while the failure mode of the corresponding fully loaded (reference) CFSST stub column specimen D73-C50 is depicted in Fig. 8.

$$\mathrm{RCI} = \frac{N_{u,p}}{N_{u,f}} \tag{2}$$

2.4. Discussion on partially and fully loaded CFSST stub column test results

2.4.1. Load-carrying capacities

The influence of the areas and shapes of the partial compression regions on the load-carrying capacities of partially loaded CFSST stub columns was discussed in this section. For each specimen series, the relative capacity indices (RCIs) are plotted against the corresponding partial compression area ratios (β) and shown in Fig. 9, indicating a clear trend that the RCI decreases as the partial compression area ratio β increases. Moreover, the RCI values are generally lower for the specimen series with smaller confinement factors ξ. For example, the RCI curves for the specimen series D73-C60-S and D73-C60-C with an average confinement factor of 0.7 lie below those for other specimen series with confinement factors ranging from 0.8 to 0.9. In addition, there have been no obvious difference between the RCI curves for the specimen series, which include the same CFSST stub columns but different shapes of partial compression regions, indicating the relative insensitivity of the load-carrying capacities of partially loaded CFSST stub columns to the shapes of partial compression regions.

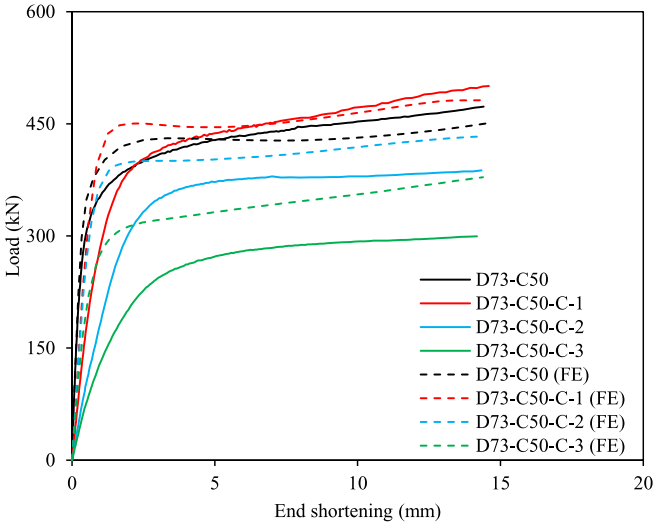

(a) Specimen series D73-C50-C.

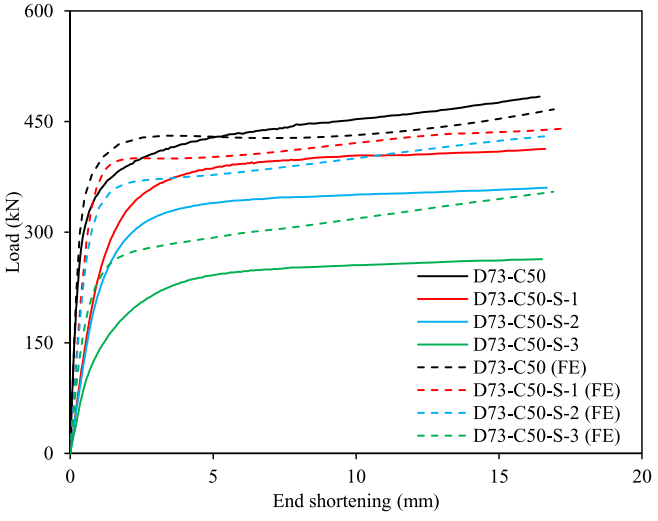

(b) Specimen series D73-C50-S.

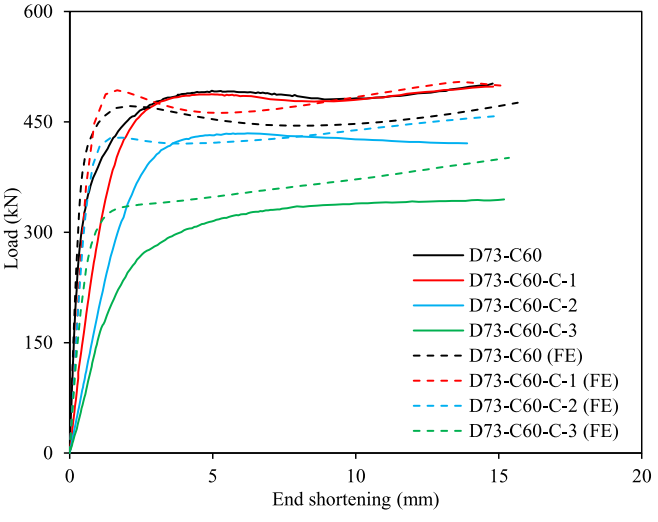

(c) Specimen series D73-C60-C.

Fig. 5. Load–end shortening curves for partially and fully loaded CFSST stub column specimens.

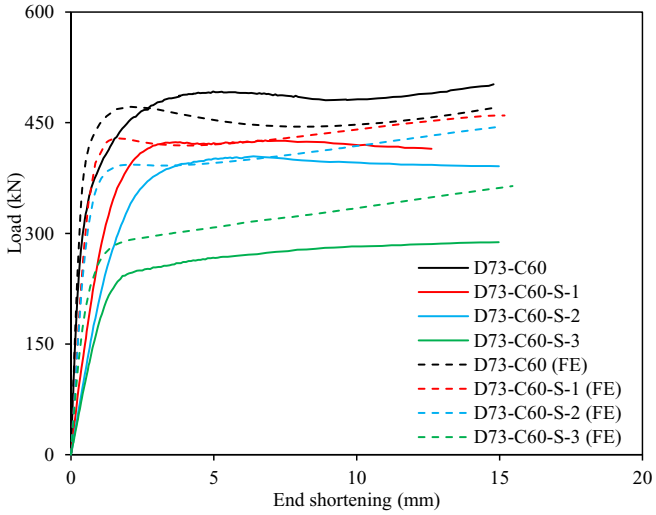

(d) Specimen series D73-C60-S.

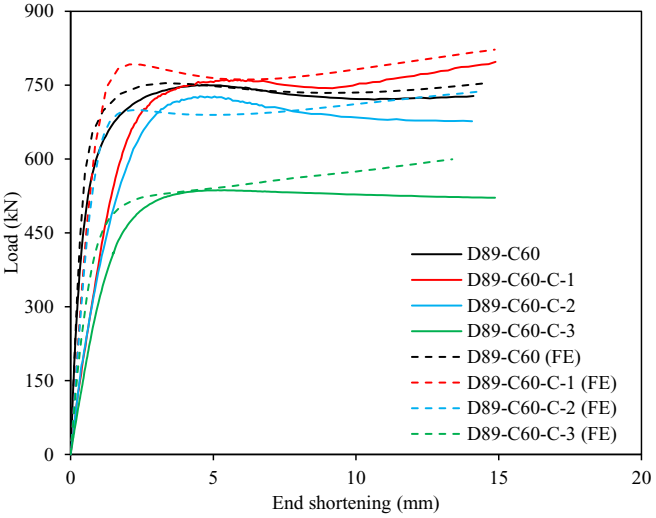

(e) Specimen series D89-C60-C.

Fig. 5 (*continued*).

2.4.2. Load–end shortening curves

The initial stiffnesses of the load–end shortening curves of the partially loaded CFSST stub columns are distinctly smaller than those of the corresponding fully loaded (reference) specimens, and are shown to reduce with increasing partial compression area ratios. It is also worth noting that the load–end shortening curves of the studied CFSST stub columns under partial and full compression exhibit more flat post-ultimate responses, compared to those from the partially and fully loaded concrete-filled carbon steel tube stub columns [27–31]; this can be attributed to the favourable material characteristics of stainless steel tubes (including high strain hardening and large ductility), which are capable of providing effective confinement to the inner concrete even after undergoing substantial deformation, thus leading to flat post-ultimate responses of partially and fully loaded CFSST stub columns.

2.4.3. Transverse and longitudinal strain distributions of stainless steel tubes

The longitudinal and transverse strain distributions of the outer stainless steel tubes along the member length direction for CFSST stub columns under partial compression were investigated in this section. Figs. 10 and 11 depict the load–strain curves measured from the three pairs of orthogonal strain gauges for typical partially loaded CFSST stub column specimens, where 'negative' and 'positive' values indicate compressive and tensile strains, respectively. It is evident in Fig. 10 that the longitudinal strain of the stainless steel tube increases as the examined point moves from the partial compression loading end to the mid-height of the specimen, with the reason being as follows: for partially loaded CFSST stub columns, the compression load was initially applied only on the concrete, and then gradually transferred to the stainless steel tube through composite action (i.e. bond strength between concrete and stainless steel tube), leading to an increasing level of compression load on the stainless steel tube (and thus longitudinal strain) along the member length direction. As depicted in Fig. 11, the transverse strain of the stainless steel tube, principally resulted from the lateral expansion of the inner concrete, tends to decrease along the member length from the end to the mid-height, which can be attributed to the reduced level of compression load on the concrete (and thus lateral expansion) along the length of the partially loaded CFSST stub column specimen.

3. Finite element simulation

3.1. General

In addition to the experimental investigation, a numerical modelling study was conducted using the finite element (FE) analysis software ABAQUS [32] in this section. Development of the partially and fully loaded CFSST stub column FE models was described in detail. The accuracy of the developed FE models was then verified through comparisons of the numerically derived results against the experimental data obtained in Section 2. On the basis of the verified FE models, parametric studies were carried out, aiming at generating further numerical results on partially loaded CFSST stub columns over a broader range of confinement factors and partial compression area ratios.

3.2. Development of FE models

FE models were developed according to the measured cross-section dimensions and lengths of the CFSST stub column specimens as listed in Table 1. The four-node shell element S4R and the eight-node brick element C3D8R [32] have been extensively adopted in previous numerical simulations [33–37] of the outer steel tubes and inner concrete cores of CFST members, respectively, and were thus also utilised herein. The sizes of the used shell element S4R and brick element C3D8R were both selected as $D/15$; this element size was found to provide not only

Table 4
Experimental ultimate loads for CFSST stub columns under partial and full compression.

Specimen	β	$N_{u,p}$ (kN)	$N_{u,f}$ (kN)	RCI
D73-C50	–	–	415	–
D73-C50-C-1	1.0	450	–	1.08
D73-C50-C-2	1.7	377	–	0.91
D73-C50-C-3	3.7	294	–	0.71
D73-C50-S-1	1.8	396	–	0.95
D73-C50-S-2	2.5	343	–	0.83
D73-C50-S-3	5.7	252	–	0.61
D73-C60	–	–	487	–
D73-C60-C-1	1.0	487	–	1.00
D73-C60-C-2	1.7	434	–	0.89
D73-C60-C-3	3.7	339	–	0.70
D73-C60-S-1	1.8	426	–	0.87
D73-C60-S-2	2.5	403	–	0.83
D73-C60-S-3	5.7	282	–	0.58
D89-C60	–	–	750	–
D89-C60-C-1	1.0	828	–	1.10
D89-C60-C-2	1.7	726	–	0.97
D89-C60-C-3	4.1	536	–	0.71

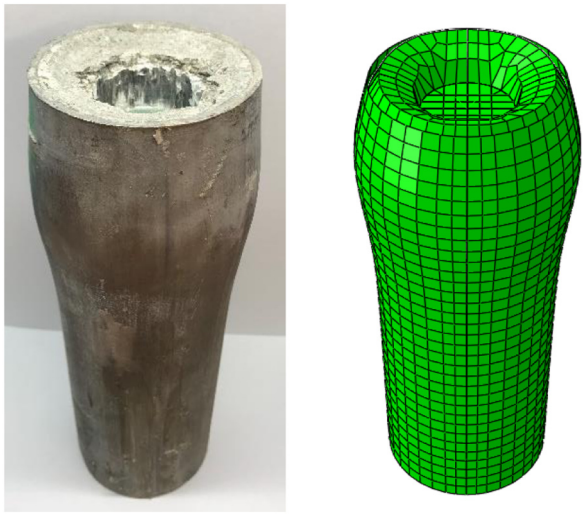

Fig. 6. Experimental and numerical failure modes for partially loaded CFSST stub column specimen D73-C50-C-3.

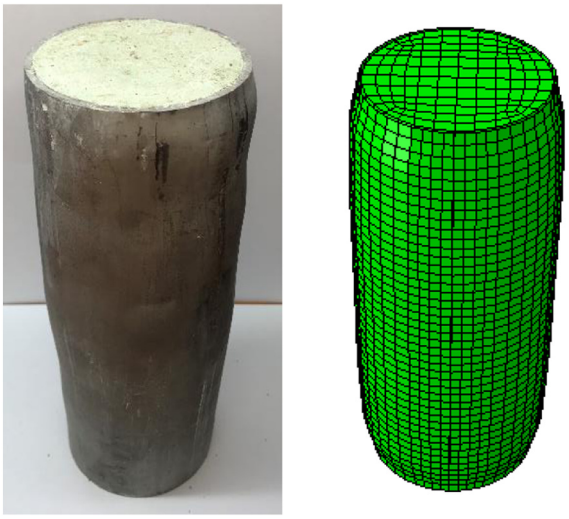

Fig. 8. Experimental and numerical failure modes for fully loaded CFSST stub column specimen D73-C50.

computational efficiency but also precise numerical results, following a mesh sensitivity study examining a range of element sizes from $D/5$ to $D/30$.

The concrete damage plasticity (CDP) model [32] was utilised to represent the material response of concrete. The modulus of elasticity of concrete was taken as $4700\sqrt{f_c}$, with the Poisson's ratio equal to 0.2, as specified in the American code ACI 318-14 [38], while the dilation angle ψ (given in Eq. (3)), flow potential eccentricity e, the ratio of the second stress invariant on the tensile meridian to that on the compressive meridian K_c, the ratio of the compressive strength under biaxial loading to the uniaxial compressive strength f_{b0}/f_c, and the viscosity parameter μ were determined, following the recommendations of Tao et al. [36]. In order to take due account of the beneficial concrete confinement effect, a confined concrete model proposed in Tao et al. [36] was utilised in the present numerical simulation to characterise the equivalent uniaxial stress–strain relationship of confined concrete in compression. With regards to the material tensile response of concrete, the relationship between stress and strain is assumed to be linear elastic up to the concrete tensile strength (taken as $0.1f_c$), beyond which an inelastic material response is characterised by means of fracture energy (G_F), as determined in accordance with the guidelines specified in CEB-FIP [39] and given by Eq. (4), where $d_{\max}$ is the maximum size of coarse aggregate and taken as 10 mm in the present study. Regarding the material modelling of stainless steel tubes, the plastic material model given in ABAQUS [32] requires the inputted material properties to be specified in the form of true stress and true plastic strain. Therefore, the measured engineering stress–strain curves were firstly converted into the true stress–true plastic strain responses and then incorporated into ABAQUS [32]. The Poisson's ratio is taken as 0.3 for stainless steel.

$$\psi = \begin{cases} 56.3(1-\xi) & \text{for } \xi \le 0.5 \\ 6.672e^{7.4/(4.64+\xi)} & \text{for } \xi > 0.5 \end{cases} \tag{3}$$

$$G_F = \left(0.0469d_{\max}^2 - 0.5d_{\max} + 26\right)\left(\frac{f_c}{10}\right)^{0.7} \tag{4}$$

The surface-to-surface contact with finite sliding has been extensively utilised to simulate the interaction behaviour between steel tubes and concrete cores in previous numerical modelling of CFST members [33–37], and was thus adopted herein. The outer surface of the

Fig. 7. Experimental and numerical failure modes for partially loaded CFSST stub column specimen D73-C50-S-2.

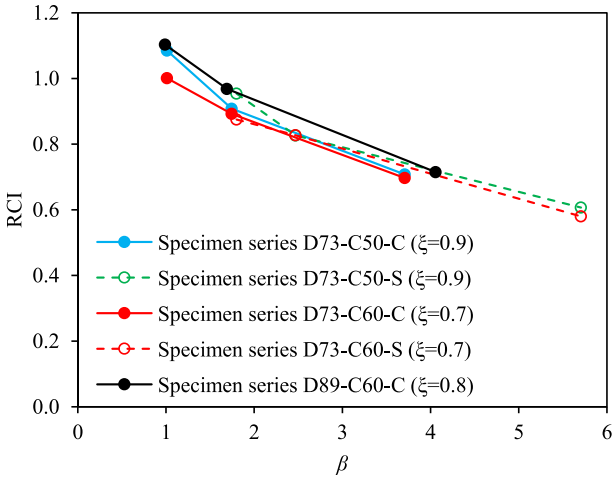

Fig. 9. Relationship between relative capacity index (RCI) and partial compression area ratio β.

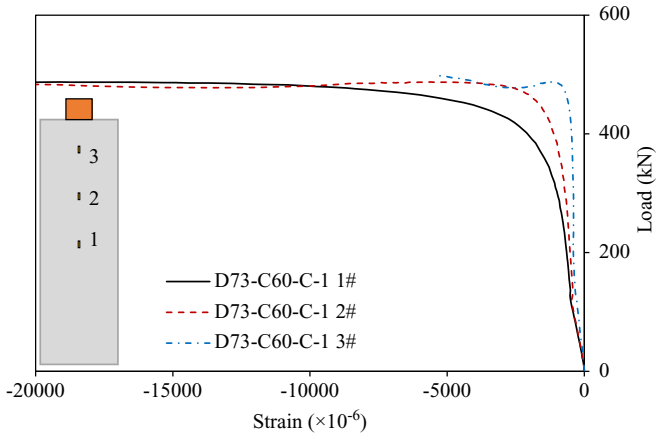

Fig. 10. Load–longitudinal strain curves for partially loaded CFSST stub column specimen D73-C60-C-1.

solid concrete core was selected as the 'master surface', while the inner surface of the thin-walled stainless steel tube was chosen as the 'slave surface'. In the normal direction, a hard contact pressure–overclosure relationship was employed, allowing the two interfaces to be separated in tension, but without penetration in compression, while the tangential behaviour between the two interfaces was defined through a penalty method with the friction coefficient set to be equal 0.25 [33].

Regarding the modelling of boundary conditions, the top (loaded) and bottom (fixed) ends of each CFSST stub column under full compression were coupled with two reference points, with all degrees of freedoms restrained except for the longitudinal translation of the top reference point. In terms of the modelling of boundary conditions for partially loaded CFSST stub columns, the bottom end section was coupled with a fully restrained reference point, while the middle portion of the top (loaded) end section was tied with a rigid plate (with the size equal to the bearing plate size used in the tests), allowing for only longitudinal translation.

3.3. Validation of FE models

Upon development of the partially and fully loaded CFSST stub column FE models, nonlinear analysis was carried out to obtain the numerical ultimate loads, load–end shortening curves and failure modes, which were then compared against the corresponding experimentally observed results, allowing the accuracy of the developed numerical models to be assessed. Table 5 reports the numerical to experimental ultimate load ratios for the partially and fully loaded CFSST stub column specimens, indicating a rather precise and consistent level of ultimate load predictions derived from finite element modelling. Fig. 5(a)–(e) show comparisons between the test and numerical load–end shortening histories for all the five specimen series. The results of the comparisons generally revealed that the shapes, ultimate loads and post-ultimate paths of the experimental load–deformation curves were all precisely captured. However, there existed a disparity between the initial slopes of the test and numerical load-end shortening curves for the partially loaded CFSST stub column specimens; this may be attributed to the existence of a weak layer of laitance on the top surface of the concrete of each specimen, resulting in larger deformation at the early stage of loading and thus smaller initial slope of the experimental load–end shortening curve compared to that derived from FE modelling. Similar disparity was also obtained in previous experimental and numerical studies of concrete-filled carbon steel tube stub columns under partial compression [28–30]. Comparisons between the experimental and numerical failure modes for typical partially and fully loaded CFSST stub column specimens are depicted in Figs. 6–8, also revealing excellent agreement. Overall, the finite element models developed herein are capable of precisely simulating the partially and fully loaded CFSST stub column tests, and thus considered to be validated.

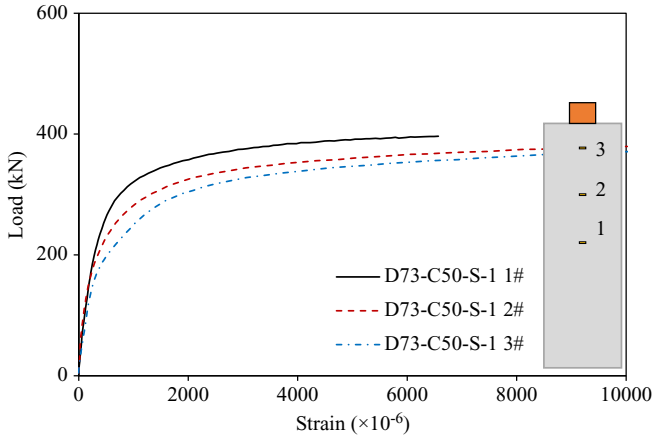

Fig. 11. Load–transverses train curves for partially loaded CFSST stub column specimen D73-C50-S-1.

3.4. Numerical parametric studies

Upon validation of the finite element models in Section 3.3, parametric studies were conducted to expand the current experimental data pool on partially loaded CFSST stub columns cover a broader range of confinement factors and partial compression area ratios. In the present numerical parametric studies, the measured material properties of CHS 89 × 3 were utilised for the outer stainless steel tubes of the modelled CFSST stub columns, while two concrete grades C50 and C60 with the measured cylinder strengths respectively equal to 49.9 MPa and 63.6 MPa were employed for the inner concrete core. With regards to the cross-section sizes, the outer stainless steel tube diameters were fixed at 100 mm, with the material thicknesses varying between 0.5 mm and 4.0 mm, leading to a broad range of confinement factors ξ from 0.1 to 1.2 being examined. Both the circular and square partial compression regions were considered, with the partial compression area ratios β ranging from 1.5 to 10.0. In total, 304 numerical parametric study results on partially loaded CFSST stub columns were generated.

4. Evaluation of existing design methods and development of new design approaches

4.1. General

In the absence of established design provisions for CFSST stub columns in partial compression, the corresponding design rules for partially loaded concrete-filled carbon steel tube stub columns, as given in the European code EN 1994-1-1 [11] and American Specification AISC 360-16 [12] and proposed by Han et al. [13], were evaluated for CFSST stub columns under partial compression load. Then, new efficient design methods were developed specifically for partially loaded CFSST stub columns, underpinned by and validated against the derived experimental and numerical results. Table 6 reports the mean ratios of the experimental and numerical failure loads to the (unfactored) predicted failure loads for all the examined design approaches $N_u/N_{u,pred}$.

Table 5
Comparison of test ultimate loads with FE ultimate loads.

Specimen	Test N_u (kN)	FE N_u (kN)	Test N_u/FE N_u
D73-C50	415	431	0.96
D73-C50-C-1	450	450	1.00
D73-C50-C-2	377	399	0.94
D73-C50-C-3	294	321	0.91
D73-C50-S-1	396	399	0.99
D73-C50-S-2	343	369	0.93
D73-C50-S-3	252	300	0.84
D73-C60	487	472	1.03
D73-C60-C-1	487	493	1.00
D73-C60-C-2	434	428	1.01
D73-C60-C-3	339	336	1.01
D73-C60-S-1	426	428	0.99
D73-C60-S-2	403	393	1.03
D73-C60-S-3	282	302	0.94
D89-C60	750	754	1.00
D89-C60-C-1	828	792	1.05
D89-C60-C-2	726	699	1.04
D89-C60-C-3	536	530	1.01
Mean			0.98
COV			0.05

4.2. EN 1994-1-1 [11] and AISC 360-16 [12]

The expressions for the calculation of load-carrying capacities of circular concrete-filled carbon steel tube columns subjected to partial compression loads applied to the concrete, as set out in the current European code EN 1994-1-1 [11] and American specification AISC 360-16 [12], follow the same format, and are given as the product of the compression resistance of the concrete within the partial compression region N_b and an enhancement factor considering the contribution from the concrete outside the partial compression region to the compression resistance k, as shown in Eq. (5). Note that both of the two design codes employ the same enhancement factor $k = \sqrt{A_c/A_b}$, but with different methods for the determination of the compression resistance of the concrete within the partial compression region N_b; the European code EN 1994-1-1 [11] accounts for the beneficial concrete confinement effect and adopts the confined concrete strength as the design strength in the calculation of N_b, while the determination of N_b in the American specification AISC 360-16 [12] was based on the unconfined concrete cylinder strength. This leads to the EC4 and AISC design formulae for partially loaded circular concrete-filled carbon steel tube stub columns given by Eqs. (6) and (7), respectively, where A_b is the area of the concrete under partial compression, A_c is the gross area of the concrete, η is a coefficient, depending on the shape of the outer steel tube, and is equal to 4.9 for circular steel tubes, f_y is the yield stress of the steel tube and f_c is the cylinder strength of the concrete. The EC4 and AISC compression resistances of partially loaded CFSST stub columns were respectively determined herein using Eqs. (6) and (7), but with $f_y = \sigma_{0.2}$, and then compared with the corresponding experimental and numerical load-carrying capacities. The mean test (or FE) to predicted resistance ratios $N_u/N_{u,pred}$ and the corresponding COVs for both design codes are presented in Table 6, indicating that the EC4 and AISC design rules for partially loaded circular concrete-filled carbon steel tube stub columns yield both conservative and scattered resistance predictions when used for circular concrete-filled stainless steel tube stub columns under partial compression, as also evident in Figs. 12 and 13, where the test and numerical load-carrying capacities are plotted against the EC4 and AISC resistance predictions, respectively.

$$N_{u,pred} = N_b k \tag{5}$$

$$N_{u,EC4} = \left(1 + \eta \frac{t}{D}\frac{f_y}{f_c}\right) f_c A_b \sqrt{\frac{A_c}{A_b}} \le f_c A_c \tag{6}$$

$$N_{u,AISC} = 0.85 f_c A_b \sqrt{\frac{A_c}{A_b}} \le 1.7 f_c A_b \tag{7}$$

4.3. Method proposed by Han et al. [13]

To address the shortcomings of the existing codified design rules in predicting the compression resistances of partially loaded circular concrete-filled carbon steel tube stub columns, Han et al. [13] developed a new design formula, based on a comprehensive regression analysis. In contrast with the form of the codified design formulae, where the load-carrying capacity of a partially loaded circular CFST stub column is equal to the compression resistance of the concrete within the partial compression region multiplied by an enhancement factor accounting for the additional compression resistance provided by the concrete outside the partial compression region, the design expression in Han et al. [13] is given as the product of the compression resistance of circular CFST stub column under full compression and a reduction factor taking into account the detrimental effect of partial compression, as shown in Eq. (8), where N_{CFST} is the cross-section compression resistance of circular CFST stub column under full compression, as determined from Eq. (9), and K_p is a reduction factor to account for the detrimental partial compression effect, and given by Eq. (10), in which A_0, B_0 and C_0 are the coefficients and derived on the basis of regression analysis, as given by Eqs. (11)–(13), respectively. The applicability of the design expression proposed in Han et al. [13] to partially loaded circular CFSST stub columns was assessed herein, through comparing the test and FE ultimate loads against the resistance predictions. The mean test (or FE) to predicted resistance ratio and the corresponding COV, as reported in Table 6, are equal to 0.93 and 0.06, respectively, indicating a high level of design accuracy and consistency of this design approach in predicting the compression resistances of partially loaded circular CFSST stub columns on average. However, it is worth noting that many of the resistance predictions are unsafe, as evident in Fig. 14, where the experimental and FE load-carrying capacities are plotted against the resistance predictions; this can be attributed to the fact that the design expression in Han et al. [13] was originally derived for concrete-filled carbon steel tube stub columns under partial compression, without specifically considering the distinct nonlinear material characteristics of stainless steel tubes.

$$N_{u,Han} = N_{CFST} K_p \tag{8}$$

$$N_{CFST} = f_c(1.14 + 1.02\xi)(A_s + A_c) \tag{9}$$

$$K_p = A_0 \cdot \frac{A_c}{A_b} + B_0 \cdot \left(\frac{A_c}{A_b}\right)^{0.5} + C_0 \tag{10}$$

$$A_0 = \left(-0.18\xi^3 + 1.95\xi^2 - 6.89\xi + 6.94\right)/100 \tag{11}$$

$$B_0 = \left(1.36\xi^3 - 13.92\xi^2 + 45.77\xi - 60.55\right)/100 \tag{12}$$

$$C_0 = \left(-\xi^3 + 10\xi^2 - 33.2\xi + 150\right)/100 \tag{13}$$

4.4. New design proposal

The existing design rules for partially loaded concrete-filled carbon steel tube stub columns were generally found to yield inaccurate resistance predictions when used for concrete-filled stainless steel tube stub columns under partial compression, which stemmed from the different material characterises of stainless steel and carbon steel tubes. This thus prompted the development of new design approaches specific for

Table 6
Comparison of test and FE results with predicted resistances.

No. of tests:18 No. of FE simulations: 304	EN 1993-1-4 [11] $N_u/N_{u,EC4}$	AISC 360–16 [12] $N_u/N_{u,AISC}$	Han et al. [13] $N_u/N_{u,Han}$	Proposed method $N_u/N_{u,pr}$
Mean value	1.60	3.54	0.93	1.10
COV	0.23	0.51	0.06	0.04

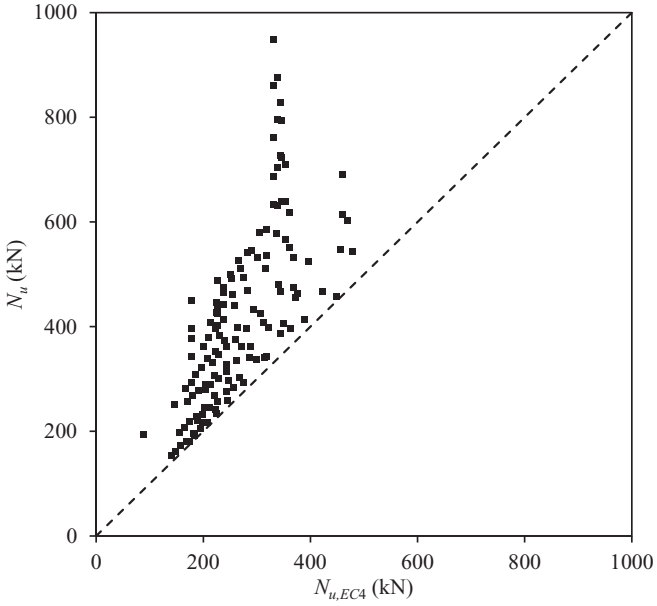

Fig. 12. Comparison of test and FE results with EN 1994-1-1 resistance predictions.

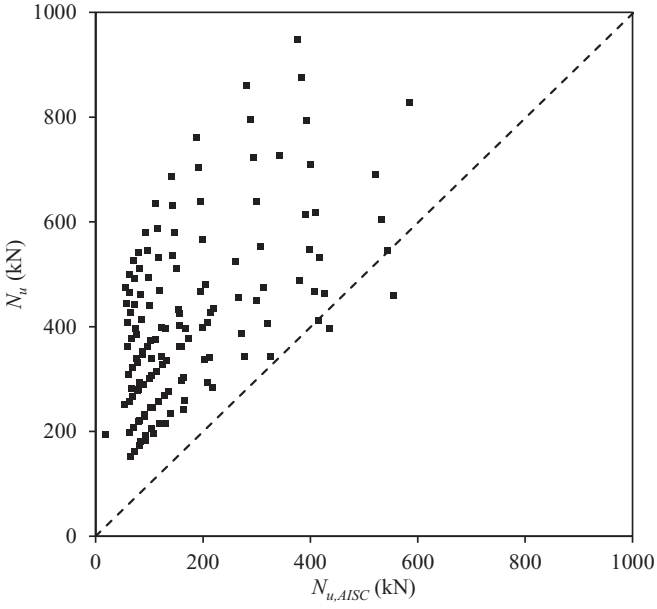

Fig. 13. Comparison of test and FE results with AISC resistance predictions.

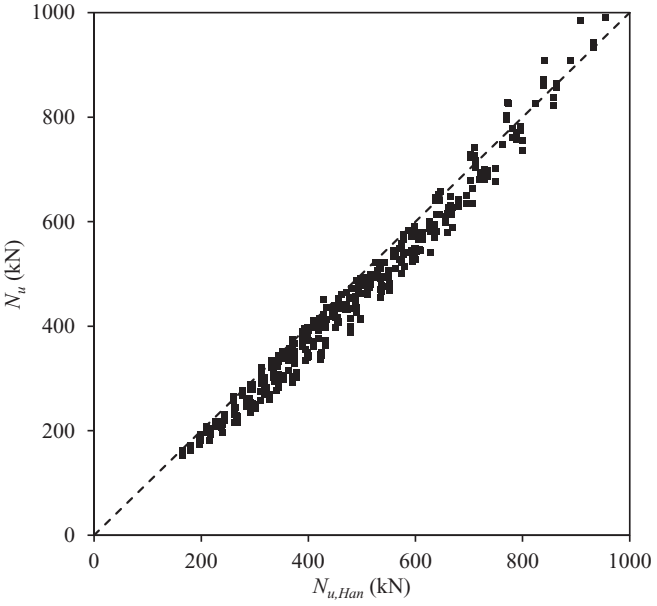

Fig. 14. Comparison of test and FE results with resistance predictions determined from the method given in Han et al. [13].

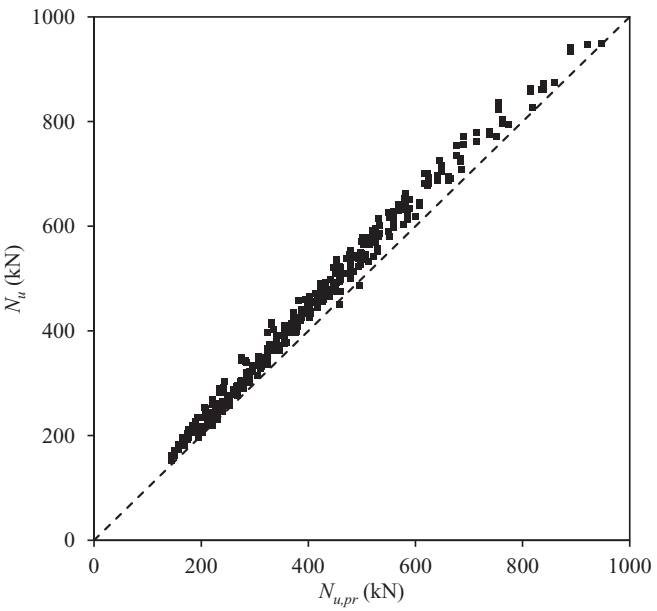

Fig. 15. Comparison of test and FE results with resistance predictions determined from the proposed method.

predicting the load-carrying capacities of partially loaded CFSST stub columns herein. The proposed design expression, as shown in Eq. (14), adopts the general form of the EC4 design formula given by Eq. (6), but with a new enhancement factor k_n derived by means of least squares regression, as given by Eq. (15). Note that the new enhancement factor is dependent on both the partial compression area ratio A_c/A_b and confinement factor ξ. The accuracy of the proposed design approach was assessed by comparing the experimentally and numerically derived load-carrying capacities of partially loaded CFSST stub columns against the resistance predictions. The mean ratio

Table 7
Comparison of test results with predicted resistances.

Specimen	Test	EC4 [11]		AISC [12]		Han et al. [13]		Proposed method	
	N_u (kN)	$N_{u,EC4}$ (kN)	$N_u/N_{u,EC4}$	$N_{u,AISC}$ (kN)	$N_u/N_{u,AISC}$	$N_{u,Han}$ (kN)	$N_u/N_{u,Han}$	$N_{u,pr}$ (kN)	$N_u/N_{u,pr}$
D73-C50-C-1	450	178	2.53	299	1.51	429	1.05	458	0.98
D73-C50-C-2	377	178	2.12	173	2.18	396	0.95	360	1.05
D73-C50-C-3	294	178	1.65	82	3.60	337	0.87	266	1.11
D73-C50-S-1	396	178	2.23	168	2.36	393	1.01	355	1.12
D73-C50-S-2	343	178	1.93	123	2.80	371	0.93	312	1.10
D73-C50-S-3	252	147	1.71	53	4.75	297	0.85	226	1.11
D73-C60-C-1	487	227	2.15	381	1.28	491	0.99	495	0.98
D73-C60-C-2	434	227	1.92	221	1.97	448	0.97	388	1.12
D73-C60-C-3	339	208	1.63	104	3.26	373	0.91	285	1.19
D73-C60-S-1	426	227	1.88	214	1.99	445	0.96	383	1.11
D73-C60-S-2	403	227	1.78	156	2.58	416	0.97	335	1.20
D73-C60-S-3	282	168	1.69	68	4.18	323	0.87	242	1.16
D89-C60-C-1	828	344	2.41	585	1.42	772	1.07	819	1.01
D89-C60-C-2	726	344	2.11	342	2.12	710	1.02	645	1.13
D89-C60-C-3	536	317	1.69	143	3.76	578	0.93	453	1.18
		Mean	1.96		2.65		0.96		1.10
		COV	0.15		0.40		0.07		0.06

of $N_u/N_{u,pr}$, as reported in Table 6, is equal to 1.10 with the COV of 0.04, revealing that the proposed method leads to precise and consistent resistance predictions for CFSST stub columns under partial compression. Moreover, all the resistance predictions lie on safe side, as displayed in Fig. 15, where the experimental and FE results are plotted against the predicted resistances. Comparisons were also made based on the experimental data only, as shown in Table 7, revealing that the new proposal yields more accurate design than the existing approaches.

$$N_{u,pr} = f_c A_b \left(1 + \eta \frac{t}{D} \frac{\sigma_{0.2}}{f_c}\right) k_n \tag{14}$$

$$k_n = 1.05\xi^{0.275} \cdot \left(\frac{A_c}{A_b}\right)^{0.689} + 0.291 \tag{15}$$

5. Conclusion

A thorough testing and numerical simulation programme has been conducted in this paper to investigate the behaviour and load-carrying capacities of circular concrete-filled stainless steel tube (CFSST) stub columns in partial compression. The testing programme was performed on 15 partially loaded circular CFSST stub column specimens and 3 fully loaded (reference) circular CFSST stub column specimens, while the finite element simulation programme included a validation study and a parametric study, where numerical models were developed to simulate the test results and to perform parametric studies to expand the experimental data pool over a broader range of partial compression area ratios and confinement factors. Given that there have been no established design rules for stainless steel-concrete composite structures, the applicability of the corresponding design rules for partially loaded concrete-filled carbon steel tube stub columns, as given in the EN 1994-1-1 [11] and AISC 360-16 [12] and proposed by Han et al. [13], to CFSST stub columns under partial compression was evaluated, on the basis of the derived test and numerical data. The two design standards [11,12] were found to lead to both conservative and scattered resistance predictions for partially loaded CFSST stub columns, while the method proposed by Han et al. [13] led to a high level of design accuracy and consistency on average, but with many unsafe resistance predictions. Finally, a new design approach was developed specifically for CFSST stub columns subjected to partial compression, and shown to yield precise, consistent and safe-sided resistance predictions through comparing against the test and FE results.

Acknowledgements

The authors would like to thank Mr. Subasanran Chelladurai, Mr. Cheng Hoon Tui and Mr. Siew Pheng Choi for their assistances in the tests. The research work described in this paper is financially support by the Academic Research Fund (AcRF) Tier 1 Grant (Project ID: 2018-T1-001-243) from the Ministry of Education, Singapore.

References

[1] B. Uy, Z. Tao, L.H. Han, Behaviour of short and slender concrete-filled stainless steel tubular columns, J. Constr. Steel Res. 67 (2011) 360–378.
[2] B. Young, E. Ellobody, Experimental investigation of concrete-filled cold-formed high strength stainless steel tube columns, J. Constr. Steel Res. 62 (2006) 484–492.
[3] D. Lam, L. Gardner, Structural design of stainless steel concrete filled columns, J. Constr. Steel Res. 64 (2008) 1275–1282.
[4] Y.-F. Yang, G.-L. Ma, Experimental behaviour of recycled aggregate concrete filled stainless steel tube stub columns and beams, Thin-Walled Struct. 66 (2013) 62–75.
[5] Y.L. Li, X.L. Zhao, R.K.R. Singh, S. Al-Saadi, Experimental study on seawater and sea sand concrete filled GFRP and stainless steel tubular stub columns, Thin-Walled Struct. 106 (2016) 390–406.
[6] Y.L. Li, X.L. Zhao, R.K. Raman Singh, S. Al-Saadi, Tests on seawater and sea sand concrete-filled CFRP, BFRP and stainless steel tubular stub columns, Thin-Walled Struct. 108 (2016) 163–184.
[7] E. Ellobody, M.F. Ghazy, Experimental investigation of eccentrically loaded fibre reinforced concrete-filled stainless steel tubular columns, J. Constr. Steel Res. 76 (2012) 167–176.
[8] L.-H. Han, F. Chen, F.-Y. Liao, Z. Tao, B. Uy, Fire performance of concrete filled stainless steel tubular columns, Eng. Struct. 56 (2013) 165–181.
[9] Z. Tao, M. Ghannam, T.-Y. Song, L.-H. Han, Experimental and numerical investigation of concrete-filled stainless steel columns exposed to fire, J. Constr. Steel Res. 118 (2016) 120–134.
[10] Y. Chen, K. He, S. Han, J. Wei, Experimental investigation of square concrete filled stainless steel tubular stub columns after exposure to elevated temperatures, Thin-Walled Struct. 130 (2018) 12–31.
[11] EN 1994-1-1:2004, Eurocode 4: Design of Composite Steel and Concrete Structures – Part 1–1: General Rules and Rules for Buildings, European Committee for Standardization (CEN), Brussels, 2004.
[12] American Institute of Steel Construction (AISC), Specification for Structural Steel Buildings, AISC 360-16, Chicago (IL), 2016.
[13] L.H. Han, W. Liu, Y.F. Yang, Design calculations on concrete-filled thin-walled steel tubes subjected to axially local compression, Proceedings of the 12th International Symposium on Tubular Structures 2008, pp. 85–91.
[14] O. Zhao, L. Gardner, B. Young, Structural performance of stainless steel circular hollow sections under combined axial load and bending – part 1: experiments and numerical modelling, Thin-Walled Struct. 101 (2016) 231–239.
[15] O. Zhao, L. Gardner, B. Young, Testing and numerical modelling of austenitic stainless steel CHS beam–columns, Eng. Struct. 111 (2016) 263–274.
[16] O. Zhao, B. Rossi, L. Gardner, B. Young, Behaviour of structural stainless steel cross-sections under combined loading – part I: experimental study, Eng. Struct. 89 (2015) 236–246.
[17] O. Zhao, B. Rossi, L. Gardner, B. Young, Experimental and numerical studies of Ferritic stainless steel tubular cross sections under combined compression and bending, J. Struct. Eng. 142 (2016), 04015110.
[18] O. Zhao, L. Gardner, B. Young, Buckling of ferritic stainless steel members under combined axial compression and bending, J. Constr. Steel Res. 117 (2016) 35–48.

[19] Y. Sun, O. Zhao, Material response and local stability of high-chromium stainless steel welded I-sections, Eng. Struct. 178 (2019) 212–226.
[20] W. Ramberg, W.R. Osgood, Description of Stress–Strain Curves by Three Parameters. Technical Note No. 902, National Advisory Committee for Aeronautics, Washington DC, 1943.
[21] H.N. Hill, Determination of stress–strain relations from offset yield strength values, Technical Note No. 927, National Advisory Committee for Aeronautics, Washington DC, 1944.
[22] E. Mirambell, E. Real, On the calculation of deflections in structural stainless steel beams: an experimental and numerical investigation, J. Constr. Steel Res. 54 (2000) 109–133.
[23] K.J.R. Rasmussen, Full-range stress–strain curves for stainless steel alloys, J. Constr. Steel Res. 59 (2003) 47–61.
[24] L. Gardner, M. Ashraf, Structural design for non-linear metallic materials, Eng. Struct. 28 (2006) 926–934.
[25] L.-H. Han, G.-H. Yao, X.-L. Zhao, Tests and calculations for hollow structural steel (HSS) stub columns filled with self-consolidating concrete (SCC), J. Constr. Steel Res. 61 (2005) 1241–1269.
[26] G.B. dos Santos, L. Gardner, M. Kucukler, A method for the numerical derivation of plastic collapse loads, Thin-Walled Struct. 124 (2018) 258–277.
[27] L.-H. Han, W. Liu, Y.-F. Yang, Behavior of thin walled steel tube confined concrete stub columns subjected to axial local compression, Thin-Walled Struct. 46 (2008) 155–164.
[28] L.-H. Han, W. Liu, Y.-F. Yang, Behaviour of concrete-filled steel tubular stub columns subjected to axially local compression, J. Constr. Steel Res. 64 (2008) 377–387.
[29] Y.F. Yang, L.H. Han, Concrete filled steel tube (CFST) columns subjected to concentrically partial compression, Thin-Walled Struct. 50 (2012) 147–156.
[30] Ding F-x, J. Liu, Liu X-m, Yu Z-w, D.-w. Li, Mechanical behavior of circular and square concrete filled steel tube stub columns under local compression, Thin-Walled Struct. 94 (2015) 155–166.
[31] Y.-F. Yang, L.-H. Han, Experiments on rectangular concrete-filled steel tubes loaded axially on a partially stressed cross-sectional area, J. Constr. Steel Res. 65 (2009) 1617–1630.
[32] ABAQUS, ABAQUS/standard user's manual volumes I–III and ABAQUS CAE manual, Version 6.12, Hibbitt, Karlsson & Sorensen, Inc, Pawtucket (USA), 2012.
[33] Z. Tao, B. Uy, F.-Y. Liao, L.-H. Han, Nonlinear analysis of concrete-filled square stainless steel stub columns under axial compression, J. Constr. Steel Res. 67 (2011) 1719–1732.
[34] L.-H. Han, G.-H. Yao, Z. Tao, Performance of concrete-filled thin-walled steel tubes under pure torsion, Thin-Walled Struct. 45 (2007) 24–36.
[35] Z. Tao, B. Uy, L.-H. Han, Z.-B. Wang, Analysis and design of concrete-filled stiffened thin-walled steel tubular columns under axial compression, Thin-Walled Struct. 47 (2009) 1544–1556.
[36] Z. Tao, Z.-B. Wang, Q. Yu, Finite element modelling of concrete-filled steel stub columns under axial compression, J. Constr. Steel Res. 89 (2013) 121–131.
[37] Y. Ye, S.-J. Zhang, L.-H. Han, Y. Liu, Square concrete-filled stainless steel/carbon steel bimetallic tubular stub columns under axial compression, J. Constr. Steel Res. 146 (2018) 49–62.
[38] American Concrete Institute, Building Code Requirements for Structural Concrete, ACI 318-14, Farmington Hills, MI, 2014.
[39] CEB-FIP (Euro-International Committee for Concrete (CEB)-International Federation for Prestressing (FIP).), Model Code for concrete structures. (CEB-FIP MC 2010), Thomas Telford, London, U.K., 2010.